ILMU KELAUTAN: Indonesian Journal of Marine Sciences *March 2025 Vol 30(1):20-30* *e-ISSN 2406-7598*

# Modeling Seasonal Variations of Sediment Transport and Morphological Changes in Delta Ecosystem: A Case Study of the Wulan Delta, Indonesia

Lintang Nur Fadlillah[1*], Margaretha Widyastuti[1], Dong Hyeon Kim [2], Muh Aris Marfai[3,4]

[1]Laboratory of Hydrology and Environmental Climatology, Faculty of Geography, Universitas Gadjah Mada
Jl. Kaliurang, Sekip Utara, Bulaksumur Sinduadi, Sleman, Daerah Istimewa Yogyakarta 55281 Indonesia
[2]East Sea Environment Research Center, East Sea Research Institute, Korea Institute of Marine Science and Technology
385 Haeyang-ro, Yeongdo-gu, Busan, South Korea
[3]Laboratory of Environmental Geomorphology and Disaster Mitigation, Faculty of Geography, Universitas Gadjah Mada
Jl. Kaliurang, Sekip Utara, Bulaksumur Sinduadi, Sleman, Daerah Istimewa Yogyakarta 55281 Indonesia
[4]Geospatial Information Agency of Indonesia
Jl. Raya Jakarta-bogor Km 46, Sentul, Cibinong, Bogor, Jawa Barat 16911 Indonesia
Email: lintang.n.f@ugm.ac.id

*Abstract*

*The suspended sediment from the Serang River plays a crucial role in the development of the Wulan Delta. This study employs the open-source DELFT3D model to investigate seasonal hydrodynamics, sediment distribution, and morphodynamic changes in the delta. Sediment dynamics during both the rainy and dry seasons were analyzed using the DELFT3D-Flow model. Tidal data were sourced from TPXO 9v1 and field measurements, while bathymetric data from GEBCO were validated against in-situ observations. Model results indicate seasonal sediment concentration patterns, which were further validated against satellite imagery, demonstrating consistency between simulated and observed sediment distribution. Statistical analysis revealed an RMSE range of 0.001 to 0.061. The estimated sediment deposition rate is approximately 1.2 t·yr* $^{-1}$*, with a deposition rate of 2.74 t·m* $^{-2}$*·yr* $^{-1}$ *at both river mouths. About 12% of the sediment accumulates near the river mouth, while the remainder is redistributed by currents influenced by the Java Sea's bed morphology. Erosion was primarily observed in the eastern part of the delta and at the OWR mouth, whereas the western delta exhibited significant deposition due to strong river currents and substantial sediment supply. This sediment distribution suggests potential delta expansion from the west to the north. Findings contribute to the understanding of sediment transport processes in deltas, with implications for mitigating coastal erosion, enhancing delta resilience, and preserving ecosystems in similar regions across northern Java.*

***Keywords:*** *DELFT3D, hydrodynamics, morphodynamics, numerical modeling, sediment transport*

## Introduction

Rapid environmental changes, driven by both global and local factors, are a pressing global concern (Mitchell *et al*., 2015; Bao and Gao, 2016). These factors, including global climate change and human activities, significantly affect coastal areas, deltas, and estuaries. Deltas, as fluvial coastlines formed through sedimentation, continually evolve under the influence of hydrodynamics and morphodynamics, reflecting a complex interplay between coastal dynamics and fluvial processes (Boudet *et al*., 2017). Dynamic processes, such as erosion, deposition, and sediment transport, are inherent to river deltas, which serve as transitional zones between fluvial and marine systems. These processes are influenced by temporal and physical conditions, including river discharge and land use changes (Nguyen *et al*., 2015; Wang *et al*., 2024).

Hydrodynamic processes not only drive morphological changes along coastlines but also affect water quality in deltas and their surrounding areas (Jiang *et al*., 2013). Building on previous research and simulation techniques, this study aims to deepen understanding of hydrodynamics, sediment transport, and their influence on delta development. Sediments transported by rivers are typically deposited at river mouths due to the interplay of hydrodynamic and morphological conditions. High sediment inputs often form micro-tidal deltaic morphologies (Renaud and Kuenser, 2012), although human interventions can significantly alter these natural processes. Upstream activities, such as aquaculture, agriculture, industry, and urban development, contribute sediment to rivers through erosion. These sediments are transported downstream, deposited in deltas, and some are eventually carried to the sea (Jalowska *et al*., 2017; Escobar *et al*., 2018).

The Wulan Delta, located in the Demak Regency of Central Java, Indonesia, lies downstream of the Serang watershed. It has evolved into an area

*) Corresponding author

https://ejournal.undip.ac.id/index.php/ijms
DOI: 10.14710/ik.ijms.30.1.20-30
Received : 04-12-2024
Accepted : 04-01-2025

characterized by aquaculture and mangrove forests. Mangroves, which partially cover the delta, are widely recognized for their critical role in hydrodynamic processes. They provide sustainable coastal protection against climate change and enhance resilience to both vertical and lateral erosion (Beselly *et al*., 2023). Despite ongoing erosion, sedimentation has led to land emergence in parts of the delta. Since its formation in 1892, the Wulan Delta has seen rapid aquaculture expansion, often on reclaimed land (Sunarto, 2008).

Several studies have investigated morphological changes (Syvitski and Saito, 2007; Sunarto, 2008; Zhang *et al*., 2015), particularly in the Wulan Delta and the northern coast of Java (Marfai *et al*., 2016; Fadlillah *et al*., 2018; Septiangga and Mutaqin, 2021). Yola *et al*. (2022) examined coastal protection design for mangrove ecosystems in the North Sea of Java using the DELFT3D model several studied has conducted research related to sediment transport outside Indonesia (Kozyrakis *et al*., 2016; Feng *et al*., 2020). However, no studies to date have focused on modeling sediment transport processes in the Wulan Delta. To address this gap, this study employs numerical modeling to investigate sediment transport and predict deltaic development. The sediment transport model specifically focuses on cohesive sediments, such as mud and silt, which are primarily transported in suspension in the area (Zhu *et al*., 2017).

Using the open-source DELFT3D model for estuarine hydrodynamics (Hasan *et al*., 2012; Kim *et al*., 2018), this study seeks to (1) Investigate seasonal hydrodynamics in the Wulan Delta and (2) Analyze suspended sediment distributions and morphodynamic changes in the Wulan Delta. This research is important to understand the process of sediment transport in delta, which most of the northern part of Java Island has similar characteristic. By identifying the depositional and erosional zone, this study provides valuable insight for mitigating coastal erosion, enhancing delta resilience, and ecological preservation in the low-lying area.

## Materials and Methods

The Wulan Delta is situated in Demak Regency, Central Java, Indonesia (Figure 1). It features two bifurcated channels: the Old Wulan River (OWR) in the North and the New Wulan River (NWR) in the South. The NWR measures 101 m wide, while the OWR measures 26 m near their mouths. The tide follows a semi-diurnal pattern with an average tidal range of 0.7-0.8 m (2007-2016), as classified by the Indonesian Agency for Meteorology, Climatology, and Geophysics Maritim (2016) and referenced by Savenji (2012) and Fadlillah *et al*. (2020).

### *Computational grid and bathymetry*

The model boundaries extend to the Java Sea from Semarang to Jepara Regency, Indonesia, covering an area of 3,899.17 km$^2$. Bathymetry data in the oceanic area were sourced from GEBCO and supplemented with field measurements conducted in January 2018 and July 2018. January and July were chosen as representative months, to represent seasonal differences. January, with the highest rainfall, is assumed to have the highest sediment input, while July, with the lowest rainfall, is expected to have the lowest sediment input. Estuary and coastal bathymetries were developed by interpolating bathymetry data from echosounder measurements taken in 2018 (Figure 1). The land boundary was digitized from Google Earth imagery dated 2018. Grids were constructed in a curvilinear manner structured grid, with greater detail near the delta (Vinh *et al*., 2016), the primary area of interest. Grid resolution ranges from 37 to 163 m near the delta, while the grids in the open ocean have a coarser resolution ranging from 1,200 to 2,555 meters. The computational grid and bathymetry are shown in Figure 1.

### *Field data collection for calibration and validation*

Field measurements of suspended sediment (SS) were conducted in January 2018 to represent the rainy season and in July 2018 to represent the dry season. SS measurements were taken during both ebb and flood tides over a 15-day tidal cycle at the New Wulan River (NWR) and Old Wulan River (OWR) (Nuraghnia *et al*., 2021). Suspended sediment samples were collected using a water sampler positioned at 0.6 of the total depth below the sea surface. Each sample was filtered through a 0.45 µm filter to determine the SS concentration. Global tide data for boundaries A, B, and C were obtained from the TPXO 9v1 global tidal model provided by Oregon State University (OSU) Poseidon Global Inverse Solution and extracted using MATLAB, meanwhile the tidal data in Station 1 and 2 were collected from Indonesian Maritime and Meteorological Agency and the Fisheries Agency were use as validation. These global tide data were used as input for the boundary conditions of the model. (Figure 2).

### *Simulation setups*

Delft3D Flow was utilized to simulate the hydrodynamics and suspended sediment transport in the Wulan Delta. The Delft3D model used in this research is the open-source mode. This numerical model is based on the shallow water equations to solve the hydrodynamics of river discharge and tides, developed by Deltares (Luan, 2017; Deltares, 2018). It employs finite difference methods (FDMs) for numerical modeling. The initial and boundary conditions for the modeling were primarily obtained from observations and collected from public data sources. Observation data include wind velocity and direction in Figure 3, whereas the input data for temperature, river discharge, salinity, and suspended sediment concentrations (SS) are presented in Table 1.

The time step for the model was set at 0.25 minutes, and the model was represented in a single layer 2D model. Manning's n was employed as the bottom roughness coefficient, set at 0.033. Wave forces stress was determined using the Fredsoe bottom stress, and horizontal eddy viscosity was fixed at 1 $m^2s^{-1}$. The initial condition for water level was set at zero relative to sea level. River stage data were obtained from automatic water level recorder (AWLR) monitoring stations (Figure 1). The model was simulated for January 2018 and July 2018. The model input setting can be seen in Table 2.

While the model is capable of considering both suspended and bed loads (Luan *et al.*, 2017), this study focuses on cohesive sediments for all scenarios, as muddy and suspended sediments are typically transported from the river, while sandy coarse sediments are often introduced from the ocean by longshore currents. The concentration of suspended sediment was determined by solving the advection-dispersion equations (Eq. 1) (Deltares, 2018).

$$\frac{\partial c^{(l)}}{\partial t}+\frac{\partial uc^{(l)}}{\partial x}+\frac{\partial vc^{(l)}}{\partial y}+\frac{\partial (w-w_s{}^{(l)})c^{(l)}}{\partial z} -\frac{\partial}{\partial x}-\left(E_{s,x}^{(l)}\frac{\partial c^{(l)}}{\partial x}\right)-\frac{\partial}{\partial y}\left(E_{s,y}^{(l)}\frac{\partial c^{(l)}}{\partial y}\right)-\frac{\partial}{\partial z}\left(E_{s,z}^{(l)}\frac{\partial c^{(l)}}{\partial z}\right)=0 \quad \text{(Eq. 1)}$$

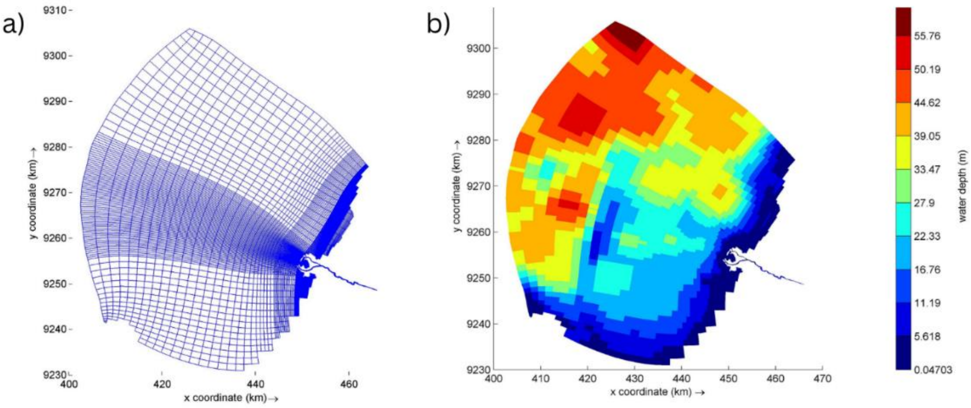


**Figure 1**. Computational grid and bathymetry of Wulan Delta using Delft3D

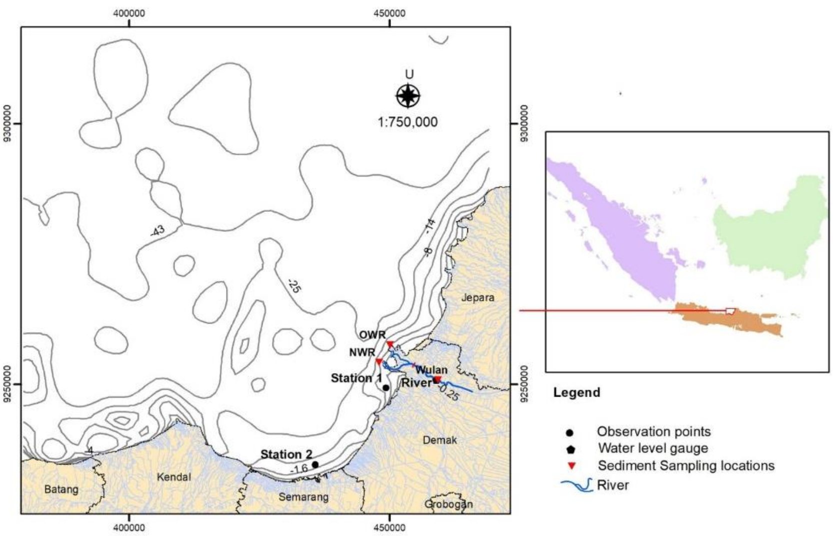


**Figure 2.** Study area location of Wulan Delta

**Table 1**. River discharge, SS, and salinity data for model boundary input

| January | | | | July | | | |
|---|---|---|---|---|---|---|---|
| Date | OWR | | | Date | NWR | | |
| | Dis ($m^3 s^{-1}$) | SS ($kg.m^{-3}$) | Sal (ppt) | | Dis ($m^3 s^{-1}$) | SS ($kg.m^{-3}$) | Sal (ppt) |
| 04/01/2018 | 369.91 | 0.47 | 0.20 | 14/07/2018 | 73.16 | 0.1413 | 15.5 |
| 05/01/2018 | 366.51 | 0.41 | 0.16 | 15/07/2018 | 70.65 | 0.2189 | 14.9 |
| 06/01/2018 | 316.53 | 0.35 | 0.20 | 16/07/2018 | 64.96 | 0.1112 | 16.6 |
| 07/01/2018 | 313.09 | 0.15 | 0.17 | 17/07/2018 | 81.69 | 0.3804 | 17.2 |
| 08/01/2018 | 309.60 | 0.48 | 0.19 | 18/07/2018 | 74.18 | 0.1908 | 16.5 |
| 09/01/2018 | 313.04 | 0.24 | 0.18 | 19/07/2018 | 69.25 | 0.3838 | 18.2 |
| 10/01/2018 | 286.00 | 0.58 | 0.27 | 20/07/2018 | 70.00 | 0.313 | 16.7 |
| 11/01/2018 | 196.56 | 0.45 | 0.26 | 21/07/2018 | 68.13 | 0.401 | 15.3 |
| 12/01/2018 | 196.75 | 0.16 | 0.22 | 22/07/2018 | 52.49 | 0.4853 | 14.6 |
| 13/01/2018 | 163.15 | 0.10 | 0.22 | 23/07/2018 | 54.37 | 0.3752 | 16.8 |
| 14/01/2018 | 209.96 | 0.07 | 0.20 | 24/07/2018 | 69.16 | 0.2661 | 16.8 |
| 15/01/2018 | 175.46 | 0.10 | 0.20 | 25/07/2018 | 63.28 | 0.1724 | 14.4 |
| 16/01/2018 | 135.71 | 0.08 | 0.21 | 26/07/2018 | 75.11 | 0.2018 | 14.4 |
| 17/01/2018 | 164.43 | 0.07 | 0.27 | 27/07/2018 | 76.78 | 0.4189 | 17.5 |
| 18/01/2018 | 166.36 | 0.06 | 0.27 | 28/07/2018 | 54.18 | 0.0825 | 15.3 |

**Table 2**. DELFT3D Model set up

| Parameter Type | Parameter Value |
|---|---|
| Simulation Time | Start: January 1st, 2018 |
| | End: July 31st, 2018 |
| Time Step | 0.25 minute |
| Bottom Roughness Formula | Manning |
| Bottom Roughness Value | 0.033 |
| Boundary Conditions | 3 Boundary Conditions |
| Water level initial condition (m) | 0 |
| Horizontal eddy viscosity ($m^2.s^{-1}$) | 1 |
| $D_{50}$ | 2.7 to 300 μm |

For non-cohesive sediment modeling, the median sediment diameter ($D_{50}$) varies from 2.7 to 300 μm, which represents clay to sand soil texture. Based on the previous research (Fadlillah *et al*., 2019), the bed sediment of Wulan River is classified as fine particles which mostly consist of sandy loam material. The critical shear stress for finer particles is hard to be determined since it strongly depends on the bulk density and particle size (Ahmad *et al*, 2011). In this research, only the suspended cohesive sediment was modeled and the bed sediment was set at a constant value size of 250 μm.

### *Model validation*

The suspended sediment model was validated by statistically comparing observed and simulated tidal and suspended sediment data using $R^2$, RMSE, and reliability (F). To evaluate the spatial variability of the suspended sediment model, we compared the simulation results with Sentinel images captured on the same dates (Vinh *et al*., 2016). The suspended sediment concentration (SS) patterns observed in the satellite images were similar to those in the model results. To ensure accuracy, atmospheric correction was applied to the satellite images using QGIS with the "Semi-Automatic Classification Plugin." The SS correction algorithm used was 5.1271 × Exp(0.0027 × Red Band). Additionally, non-water objects were masked using the Normalized Difference Vegetation Index (NDVI) for the January image and the Normalized Difference Water Index (NDWI) for the July images. These image processing techniques were implemented to align the satellite-derived SS values with the observed suspended sediment transport values

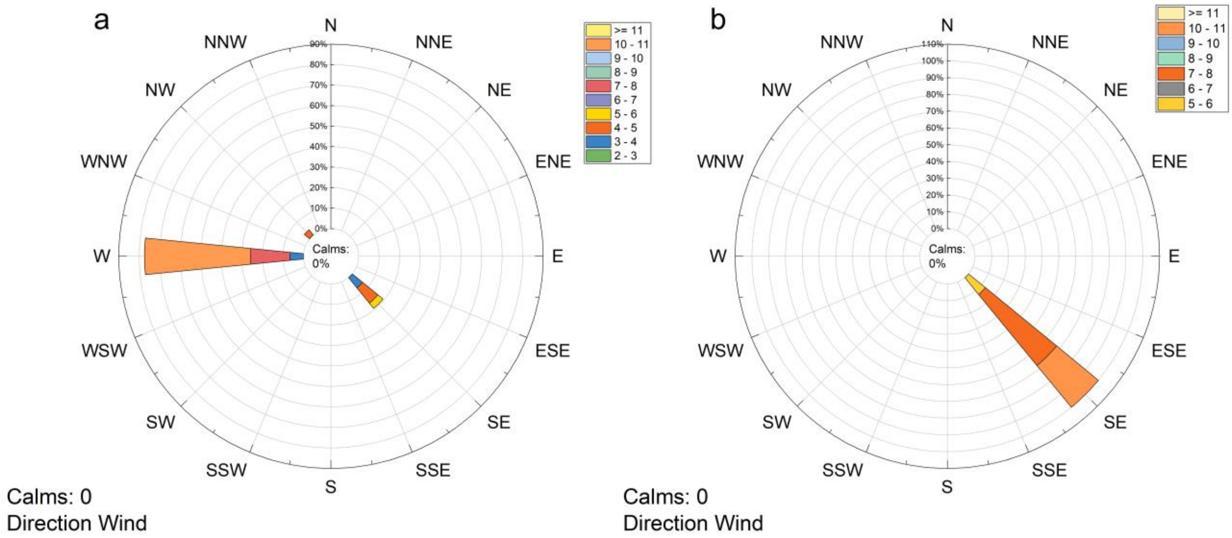


**Figure 3**. Wind direction for model input

## Result and Discussion

### *Water level model*

Tides were simulated with four specific tidal constituents, including M2, O1, K1, and S2, as the dominant constituents in the Java Sea. To calibrate the tidal model, sea levels were compared to observational data at two locations: Station 1 (49 M, 449313.02 m E, 9249256.79 mS) and Station 2 (49 M, 434857.93 m E, 9238183.79 mS) (see Figure 1). Comparisons of the observational and simulated water level data demonstrate reasonable performance at both stations (see Figure 4). The amplitudes of each constituent have errors ranging from 0.6 to 3.1 cm in January and 0.1 to 1.5 cm in July. Whereas the phase errors were in varied from 2.47° to 38.6° for January and 0.99° to 29.6° for July. Table 3 illustrates a phase-lag error of approximately 15-20% between the observational data and simulation data. This difference can be attributed to the use of global bathymetry from GEBCO, which contributes errors to the model results. However, this issue cannot be overlooked due to the limited data available for the study area. To minimize this discrepancy, downscaled bathymetric data were obtained using field measurements. Despite this, the 15-20% error remains within an acceptable range. Therefore, even though K1, which has the largest amplitude among the four constituents, exhibits amplitude errors smaller than 10%, these errors are still considered acceptable. Similar amplitude errors were observed in a study conducted in Jepara, Indonesia (Atmodjo, 2016).

### *Seasonal Suspended Sediment Model Calibration*

During the calibration process, three statistical indicators exhibited high agreement between the observed Suspended Sediment Concentration (SS) for both the rainy season and dry season. As depicted in Table 4, the average values of R2, RMSE, and the reliability statistic (F) for the rainy season are 0.96, 0.017, and 1.13, respectively. The reliability statistic was derived from the correlation between observed and simulated sediment concentration using a reliability coefficient formula. It serves to evaluate and compare the suitability and compatibility of the model with actual conditions (Yang *et al*., 2016). The calibration the model conducted by comparing the model simulation with observational data show a good statistical number (Lee *et al*., 2018). Table 4 and can be accepted for simulation. Figure 5 represent the graph of simulated and observed SS.

### *Suspended sediment model from DELFT-3D*

The output model for hydrodynamic and suspended sediment concentration distribution in the Wulan Delta during the rainy and dry seasons are represent in Figure 6 and 7 illustrates. Figure 6 depict snapshots of the model during the rainy season (January 2018), while Figure 7 represent the dry season (July 2018). During peak flow in the rainy season, suspended sediment can extend up to 2 km offshore from the NWR mouth. Simulated SS values near the NWR mouth ranged from 0.048 to 0.67 $kg.m^{-3}$, while those near the OWR mouth were relatively lower, ranging from 0.072 to 0.674 $kg.m^{-3}$. In contrast, during the dry season's low-flow conditions, sediment dispersal from the river mouth reached up to 1 km offshore at the NWR, with maximum SS values of 0.42 kg.m$^{-3}$ at the NWR and 0.24 kg.m$^{-3}$ at the OWR.

Satellite images were used to validate the sediment transport model on corresponding dates shown in Figure 8. These images generally matched the simulated SS patterns. However, the satellite

**Table 3**. Observed and Simulated Amplitude and Phase

| Tidal Constituent | January Amplitude | | July Amplitude | | January Phase | | July Phase | |
|---|---|---|---|---|---|---|---|---|
| | observation (cm) | simulation (cm) | observation (cm) | simulation (cm) | observation (°) | simulation (°) | observation (°) | simulation (°) |
| Station 1 | | | | | | | | |
| M2 | 9.7 | 9.1 | 8.5 | 8.4 | 231.34 | 249.3 | 230.08 | 200.48 |
| O1 | 7.8 | 7.2 | 7.2 | 6.3 | 178.34 | 183.05 | 175.23 | 146.37 |
| K1 | 18.9 | 20.9 | 20.1 | 21.6 | 353.02 | 336.1 | 350.91 | 344.9 |
| S2 | 6.6 | 5.6 | 6.6 | 7.2 | 155.78 | 163.93 | 149.6 | 145.62 |
| Station 2 | | | | | | | | |
| M2 | 9.7 | 9.8 | 8.5 | 8.4 | 231.34 | 192.65 | 195.47 | 200.52 |
| O1 | 6.6 | 7.2 | 7 | 6.4 | 178.34 | 175.87 | 127.53 | 140.76 |
| K1 | 24.2 | 22.1 | 21.6 | 21.5 | 353.02 | 347.17 | 343.77 | 344.76 |
| S2 | 3.5 | 4.5 | 6.9 | 7.3 | 155.78 | 158.72 | 123.61 | 144.7 |

**Table 4**. Statistical analysis of simulated and observed values of suspended sediment

| Event | Location | $R^2$ | F | RMSE |
|---|---|---|---|---|
| Rainy Season | Old Wulan River | 0.93 | 1.28 | 0.005 |
| | New Wulan River | 0.98 | 1.29 | 0.061 |
| Dry Season | Old Wulan River | 0.97 | 0.95 | 0.001 |
| | New Wulan River | 0.99 | 1.02 | 0.003 |

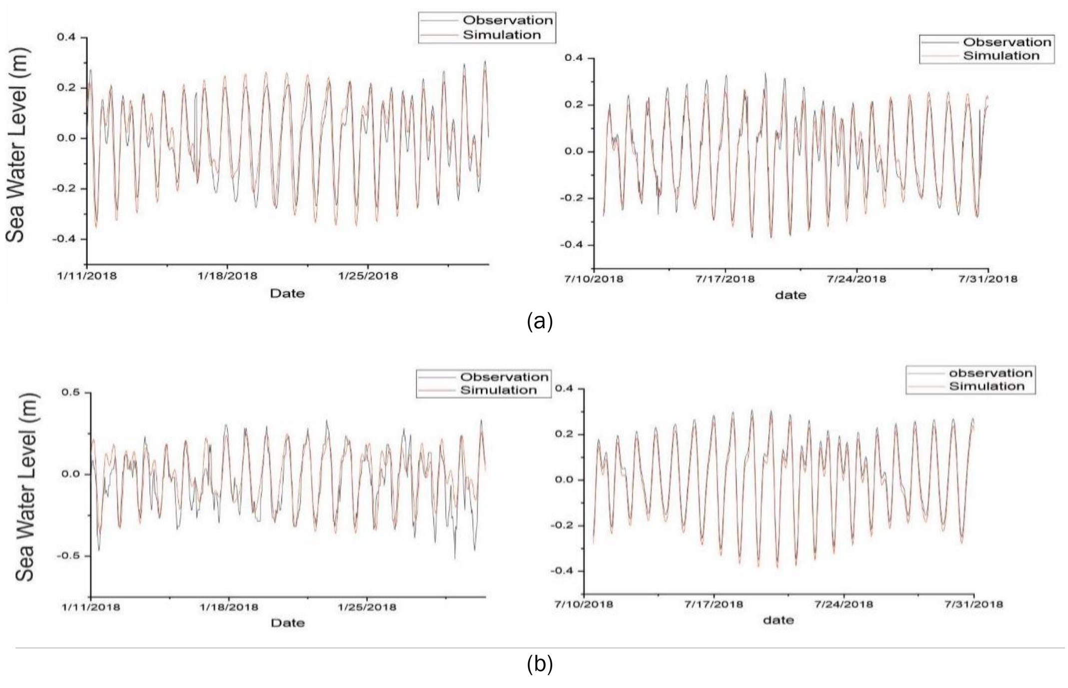


**Figure. 4**. Simulated sea level compared with observations in January and July at Station 1 (a) and Station 2 (b)

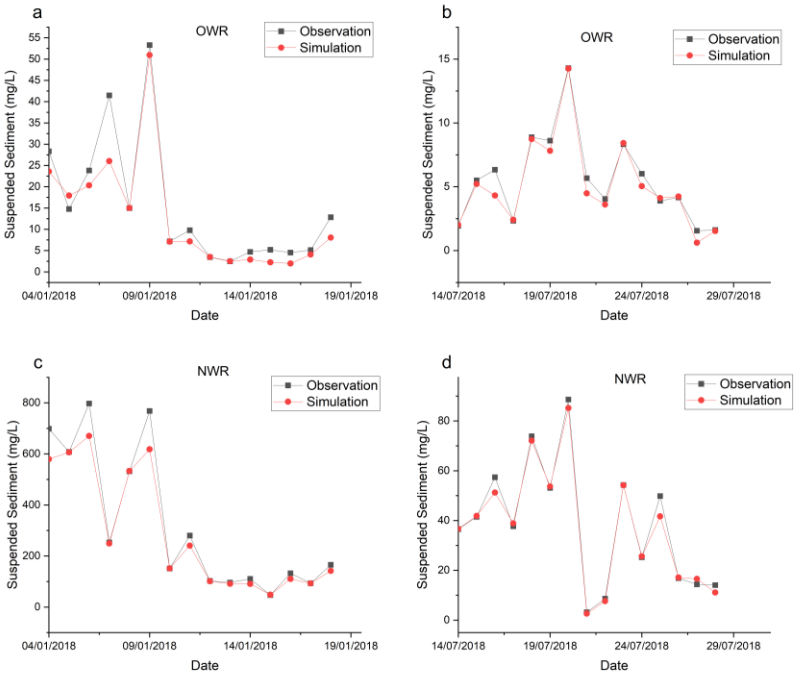


**Figure. 5.**Model performance of observed and simulated sediment concentration in January and July for both New Wulan River (NWR) mouth and Old Wulan River (OWR) mouth

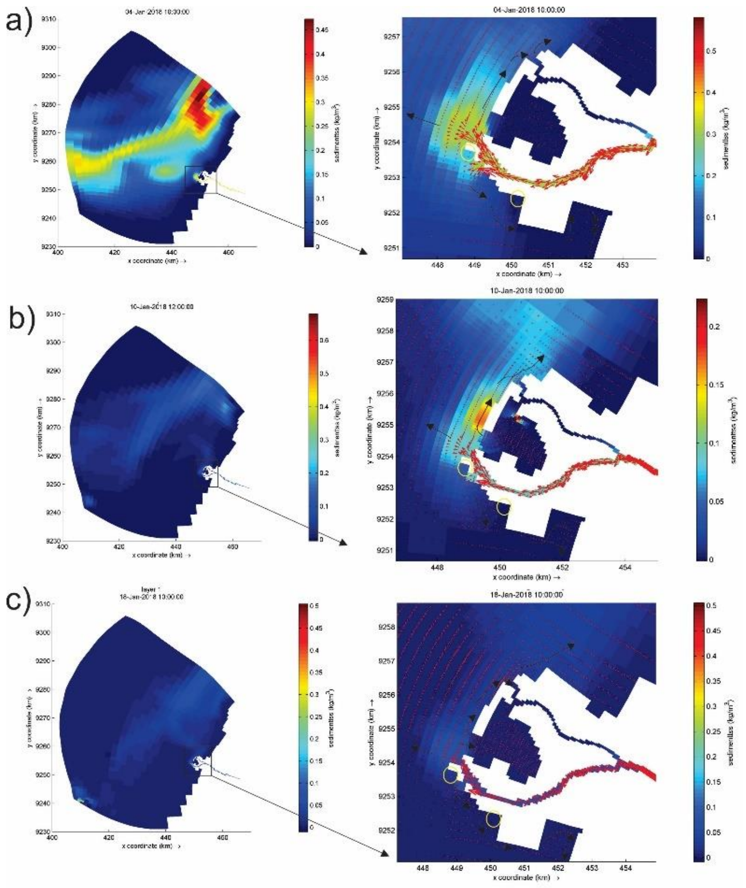


**Figure 6**. Snap shot of suspended sedimen in January

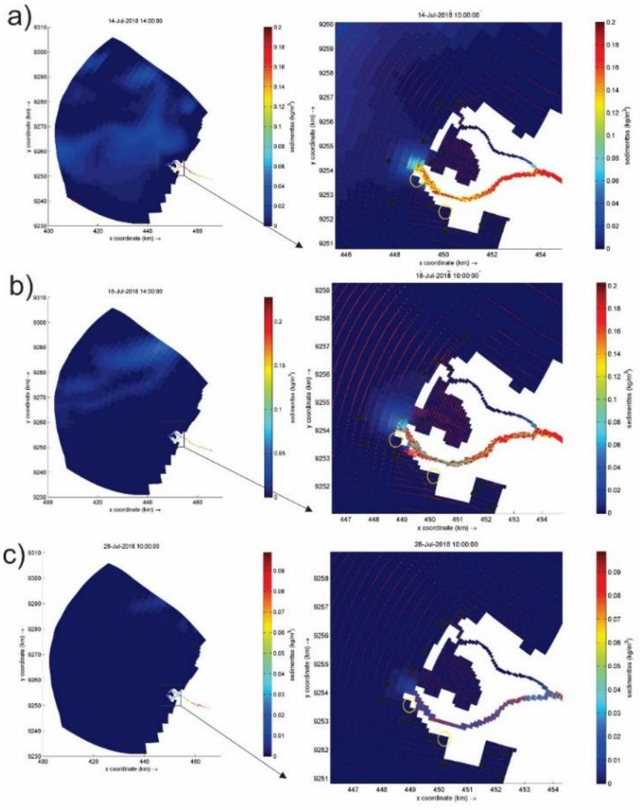


**Figure 7**. Snap shot of suspended sedimen in January

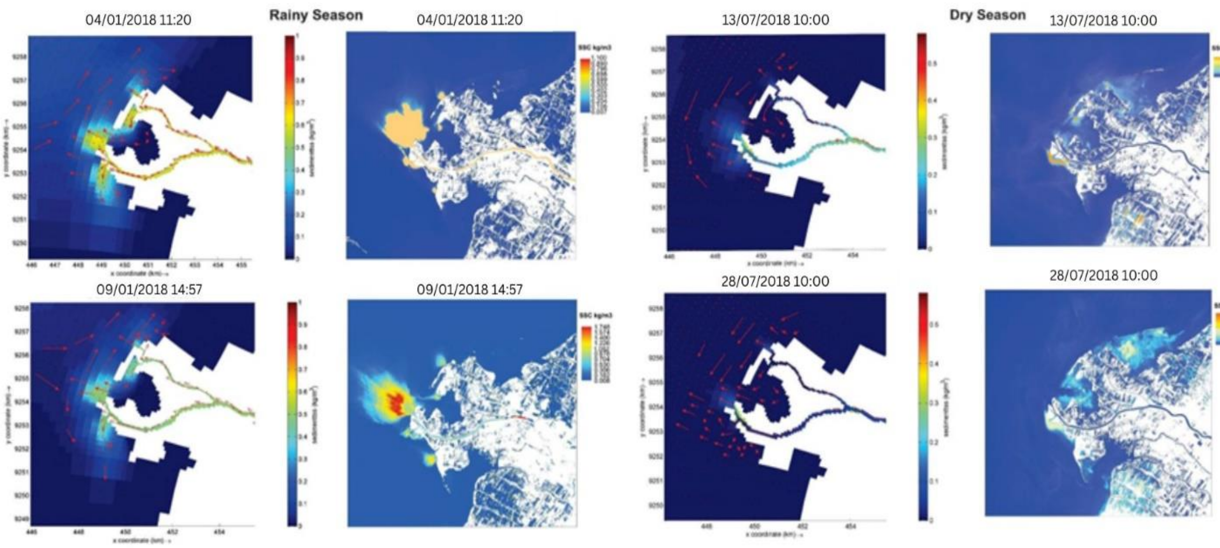


**Figure 8**. Spatial distribution of simulated suspended sediment concentration from the numerical modelling (left) and sentinel satellite image collected and corrected into SS in kg.m$^{-3}$ (right) in Rainy Season and dry season

image from January 9, 2018, exhibited an overestimation of Suspended Sediment, which hindered the differentiation between SS in water and land, thereby affecting the correction process (Hariyanto *et al*., 2017). The estimated sediment load from the NWR and OWR rivers is approximately 1.2 t·yr$^{-1}$, with a deposition rate of 2.74 t·m$^{-2}$·yr$^{-1}$ at both river mouths. This results in an estimated delta growth of 594,980.19 m$^{2}$.yr$^{-1}$, excluding the effects of flocculation, remixing, and transportation. The

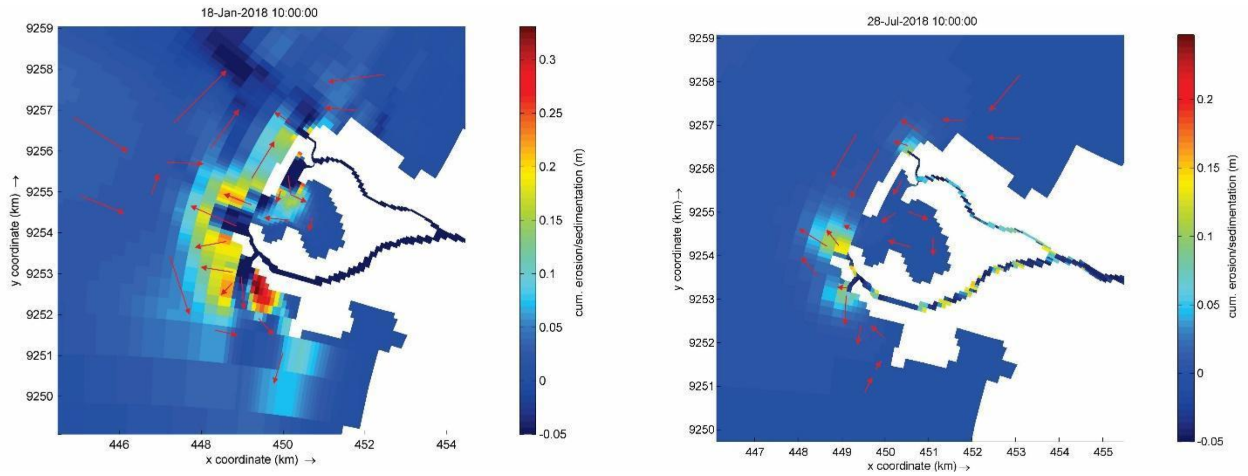


**Figure 9.** Snapshot Cumulative erosion and sedimentation from DELFT 3D Model

hydrodynamic settings of the micro-tidal environment are relatively complex, requiring enhanced model sensitivity (Pappas *et al*., 2023).

### *Morphodynamic changes*

Morphodynamic changes in the Wulan Delta, driven by hydrodynamic processes, further illustrate the interplay between erosion and sedimentation patterns as model and validated. Cumulative erosion and sedimentation patterns, as shown in Figure 9 highlight the distinct seasonal variations. Positive values represent zones of sedimentation, while negative values denote eroded zones (Zhu *et al*., 2017). During January (rainy season), significant bed erosion occurred within the river due to high river flow velocities, with erosion variations of approximately 0.05 meters (Luan *et al*., 2017). Sediment deposition was concentrated near the river mouth and its surroundings, with cumulative sedimentation reaching up to 0.3 m by the end of January. Deposition zones were predominantly located around the NWR mouth and the western delta, with sediment accumulation ranging from 10 to 35 cm. Conversely, the July (dry season) simulations showed smaller sedimentation values, ranging from 5 to 25 cm, as river flow discharge was reduced and tidal energy dominated. Depositional zones in the dry season were observed before the delta bifurcation and along the NWR and OWR channels, highlighting areas potentially suitable for mangrove plantations to mitigate river erosion of nearby aquaculture areas. These seasonal morphodynamic changes emphasize the complexity of hydrodynamic and sediment transport processes in micro-tidal environments, aligning with the model's reliability and statistical performance as previously described.

### *Model limitations*

The limitation of this research was that, although the model was input with data from different scales that needed to be downscaled, the sediment model demonstrated an error of less than 23%, while the tidal model had an error of approximately 10%. However, the DELFT3D Flow model results proved to be a reliable hydrodynamic and sediment transport model indicated by good statistical results and satellite imagery validation, which show similar results to satellite image and previous research conducted in study area (Sunarto, 2008; Septiangga and Mutaqin, 2021), highlighting the Wulan Delta's developmental trajectory toward the west and north. Satellite data can serve as a valuable complement for validating the outcomes of the model (Vinh *et al*., 2016). Moreover, the computational model's validation against satellite imagery identifies the eastern part of the delta as a vulnerable area to coastal erosion. While this region is suitable for mangrove plantation to mitigate erosion, it is also exposed to strong waves and currents, posing a risk of mangrove destruction (Van *et al*., 2021; Xie *et al*., 2022).

## Conclusion

In conclusion, this research successfully simulated both tidal and suspended sediment processes in the Wulan Delta. The calibration of the tidal model, showed good accuracy, with amplitude errors ranging from 0.6 to 3.1 cm in January and 0.1 to 1.5 cm in July, and phase errors between 2.47° to 38.6° in January and 0.99° to 29.6° in July. Despite these challenges, the model's performance was consistent with previous regional studies and demonstrated a strong correlation between observed and simulated sediment concentrations ($R^2$= 0.93–

0.99) with error margins of <23% for sediment transport and ~10% for tidal modeling. The seasonal variation showed widespread sediment dispersal extended up to 2 km offshore during rainy season, bu was restricted to 1 km in the dry season. Satellite imagery confirmed delta expansion toward the west and north, consistent with model results. Overall, the DELFT3D Flow model proved to be a robust tool for simulating tidal and sediment transport processes in complex estuarine systems like the Wulan Delta. These results offer valuable contributions to understanding delta dynamics and will support future efforts in delta management and coastal protection strategies.

## Acknowledgement

We would like to acknowledge Prof. Dr Sunarto, M.S. who is one the of project members for all his contributions and support to this research formerly. We also thank Prof. Hwang Jin Hwan from Seoul National University for his advice and contribution to this manuscript.

## References

Ahmad, M.F., Dong, P., Mamat, M., Nik, W.B.W. & Mohd, M.H. 2011. The critical shear stress for sand and mud mixture. *Appl. Math. Sci.*, 5(2): 53-71.

Atmodjo, W. 2016. Geomorfologi pesisir pantai Benteng Portugis, Kecamatan Donorejo, Kabupaten Jepara. *J. Kelaut. Trop.*, 19(2): 150-160. https://doi.org/10.14710/jkt.v19i2.842

Bao, J. & Gao, S. 2016. Environmental characteristics and land-use pattern changes of Old Huanghe River Delta, Eastern China, in the sixteenth to twentieth centuries. *Sustain. Sci.*, 11: 695-709. https://doi.org/10.1007/s11625-016-0365-5

Beselly, S.M., Grueters, U., Der Wegen, M., Reyns, J., Dijkstra, J. & Roelvink, D. 2023. Modelling mangrove-mudflat dynamics with a coupled individual-based-hydro-morphodynamic model. *Environ. Model. Softw.*, 169: 105814. https: //doi.org/10.1016/j.envsoft.2023.105814

Boudet, L., Sabatier, F. & Radakovitch, O. 2017. Modeling of sediment transport pattern in the mouth of the Rhone delta: Role of storm and flood events. *Estuar. Coast. Shelf Sci.*, 198: 568-582. https://doi.org/10.1016/j.ecss.2016.10.004

Deltares. 2018. Delft3D-Flow user manual. Delft: Deltares.

Escobar, C.A. & Montoya, L.V. 2018. Modelling the sediment dynamics in the Gulf of Uraba, Colombian Caribbean Sea. *Ocean Eng.*, 147: 476-487. https://doi.org/10.1016/j.oceaneng.2017.10.055

Fadlillah, L.N., Sunarto, Widyastuti, M. & Marfai, M.A. 2018. The impact of human activities in the Wulan Delta estuary, Indonesia. *IOP Conf. Ser.: Earth Environ. Sci.*, 148: 1-10. https://doi.org/10.1088/1755-1315/148/1/012032

Fadlillah, L.N., Widyastuti, M., Geottongsong, T., Sunarto & Marfai, M.A. 2019. Hydrological characteristics of estuary in Wulan Delta in Demak Regency, Indonesia. *Water Resour.*, 46(6): 832-843. https://doi.org/10.1134/S0097807819060101

Fadlillah, L.N., Widyastuti, M., Sunarto & Marfai, M.A. 2020. Comparison of tidal model using MIKE21 and Delft3D-Flow in part of Java Sea, Indonesia. *IOP Conf. Ser.: Earth Environ. Sci.*, 451: 1-7. https://doi.org/10.1088/1755-1315/451/1/012067

Feng, H., Tang, L., Wang, Y., Guo, C., Liu, D., Zhao, H., Zhao, L. & Wang, W. 2020. Effects of recent morphological change on the redistribution of flow discharge in the Yangtze River Delta. *Cont. Shelf Res.*, 208: 104218. https://doi.org/10.1016/j.csr.2020.104218

Guo, C., He, Q., Guo, L. & Winterwerp, J.C. 2017. A study of in-situ sediment flocculation in the turbidity maxima of the Yangtze Estuary. *Estuar. Coast. Shelf Sci.*, 191: 1-9. https://doi.org/10.1016/j.ecss.2017.04.001

Hariyanto, T., Krisna, T.C., Khomsin, Pribadi, C.B. & Anwar, N. 2017. Development of total suspended sediment model using Landsat-8 OLI and in-situ data at the Surabaya Coast, East Java, Indonesia. *Indones. J. Geogr.*, 49(1): 73-79. https://doi.org/10.22146/ijg.12010

Hasan, G.M.J., van Maren, D.S. & Cheong, H.F. 2012. Improving hydrodynamic modeling of an estuary in a mixed tidal regime by grid refining and aligning. *Ocean Dyn.*, 62: 295-409. https://doi.org/10.1007/s10236-011-0506-4

Jiang, A.W., Ranasinghe, R. & Cowell, P. 2013. Contemporary hydrodynamics and morphological change of a microtidal estuary: A numerical modelling study. *Ocean Dyn.*, 63: 21-41. https://doi.org/10.1007/s10236-012-058 3-z

Kim, N.H., Hwang, J.H., Cho, J. & Kim, J.S. 2018. A framework to determine the locations of the environmental monitoring in an estuary of the Yellow Sea. *Environ. Pollut.*, 241: 576-585. https://doi.org/10.1016/j.envpol.2018.05.097

Kozyrakis, G., Delis, A., Alexandrakis, G. & Kampanis, N. 2016. Numerical modeling of sediment transport applied to coastal morphodynamics. *Appl. Numer. Math.*, 104: 30-46. https://doi.org/10.1016/j.apnum.2014.09.007

Luan, H.L., Ding, P.X., Wang, B.Z. & Ge, J.Z. 2017. Process-based morphodynamic modeling of the Yangtze Estuary at a decadal timescale: Controls on estuarine evolution and future trends. *Geomorphology*, 290: 347-364. https://doi.org/10.1016/j.geomorph.2017.04.016

Marfai, M.A., Tyas, D.W., Nugraha, I., Ulya, A.F. & Riasasi, W. 2016. The morphodynamics of Wulan Delta and its impact on the coastal community in Wedung Sub-district, Demak Regency, Indonesia. *J. Environ. Prot.*, 7: 60-71. https://doi.org/10.4236/jep.2016.71006

Mitchel, S.B., Jennerjahn, T.C., Vizzini, S. & Zhang, W. 2015. Changes to processes in estuaries and coastal waters due to intense multiple pressures-an introduction and synthesis. *Estuar. Coast. Shelf Sci.*, 156: 1-6. https://doi.org/10.1016/j.ecss.2014.12.027

Syvitski, J.P. & Saito, Y. 2007. Morphodynamics of deltas under the influence of humans. *Glob. Planet. Change*, 57(3–4): 261-282. https://doi.org/10.1016/j.gloplacha.2006.12.001

Wang, J., Chu, A., Dai, Z. & Nienhuis, J. 2024. Delft3D model-based estuarine suspended sediment budget with morphodynamic changes of the channel-shoal complex in a mega fluvial-tidal delta. *Eng. Appl. Comput. Fluid Mech.*, 18(1): 2300763. https://doi.org/10.1080/19942060.2023.2300763

Winterwerp, J.C., Albers, T. & Anthony, E. J. 2020. Managing erosion of mangrove-mud coasts with permeable dams – lessons learned. *Ecological Engineering,* 158: 106078. https://doi.org/10.1016/j.ecoleng.2020.106078

Xie, D., Schwarz, C., Kleinhans, M.G., Zhou, Z. & van Maanen, B. 2022. Implications of coastal conditions and sea-level rise on mangrove vulnerability: A bio-morphodynamic modeling study. *J. Geophys. Res. Earth Surf.,* 127: e2021JF006301. https://doi.org/10.1029/2021JF006301

Yang, Y., Yin, X., & Yang, Z. 2016. Environmental flow management strategies based on the integration of water quantity and quality: A case study of the Baiyangdian Wetland, China. *Ecol. Eng.,* 96: 150–161. https://doi.org/10.10 16/j.ecoleng.2015.12.018

Yola, Y.N., Kurniawan, A., Nugroho, E.O., Martin, R.J., Muhammad, I.F., Wijaya, F.S. & Fauzi, N. 2022. Coastal protection system design at the Indonesian Mangrove Center in Pekalongan, Central Java – Indonesia. *IOP Conf. Ser. Earth Environ. Sci.,* 1065(1): p.012062. https://doi.org/10.1088/1755-131 5/1065/1/012062

Zhu, Q., Wang, Y. P., Gao, S., Zhang, J., Li, M., Yang, Y. & Gao, J. 2017. Modeling morphological change in anthropogenically controlled estuaries. *Anthropocene,* 17: 70–83. https://doi.org/10.1016/j.ancene.2017.03.001

Zhang, W., Xu, Y., Hoitink, A., Sassi, M., Zheng, J., Chen, X., & Zhang, C. 2015. Morphological change in the Pearl River Delta, China. *Mar. Geol.,* 363: 202–219. https://doi.org/10.1016/j.margeo.2015.02.012